ESOMAT 2009, 03003 (2009)
DOI:10.1051/esomat/200903003

Modeling of shape-memory alloys on the mesoscopic level

Barbora Benešová[a]

Institute of Thermomechanics of the ASCR, Dolejškova 5, 18200 Prague 8, Czech Republic

Abstract. This contribution presents some recent results on modeling of phase transformation in the pseudo-elastic regime within the framework of continuum mechanics. We recall an efficient concept for quasi-static evolution of microstructure in the isothermal rate-independent case. We then concentrate on simulation results obtained by the presented model, performed on a single-crystal prismatic $NiTi$-specimen. Algorithmic details, i.e. energy-estimates-based optimization, are also given.

1 Introduction, Gibbs free energy, Dissipation, Energetic Solutions

Shape-memory alloys (abbreviated SMA) are smart materials exhibiting special features due to their solid-to-solid phase transition (the so-called martensitic transition). Because of that, they have been in the scope of experimental as well as analytical and computational research for decades cf. [1,3–5,9,21,22,24,30].

In this contribution we describe the behavior of SMA on the mesoscopic level, i.e. the main description tool is continuum mechanics, but combined with multiscale modeling. This approach is outlined also in e.g. [3,5,22], for a comparison of different models see e.g. [27].

We consider the stress-free austenite, being a bounded Lipschitz domain $\Omega \subset \mathbb{R}^3$, as reference configuration. Any smooth injective function $y(t) : \Omega \to \mathbb{R}^3$ such that $\det\nabla y(x,t) > 0$ is called a *deformation* of the body.

The mechanical response of the material is modeled by constitutively specifying the stored energy $\varphi(\nabla y)$ (in fact $\varphi(F) = \tilde{\varphi}(\nabla y^T \nabla y)$ to assure frame-indifference). When modeling SMA, it is necessary to choose the stored energy to be of a multi-well character (see e.g. [4,5,21]), the wells corresponding to the variants of martensite and austenite. Due to the multi-well character of the stored energy the infimizing sequences of the stored energy tend to develop fast spatial oscillations, the so called *microstructure*, which can be effectively described by means of *gradient Young measures* (see [3,4,21]), for more information on Young measures see e.g. [23]. Those are probability measures $x \mapsto \nu_x$ that are attained by gradients in the following sense: For every $g \in L^\infty(\Omega,\mathbb{R})$, every $\psi : \Omega \times \mathbb{R}^{3\times 3} \mapsto \mathbb{R}$ Carathéodory function, and every bounded sequence $\{u_k\}_{k=0}^\infty \in W^{1,p}(\Omega,\mathbb{R}^3)$ such that $\{\psi(x,\nabla u_k)\}_{k=0}^\infty$ is weakly convergent in $L^1(\Omega,\mathbb{R})$ it holds (at least for a sub-sequence) $\lim_{k\to\infty} \int_\Omega g(x)\psi(x,\nabla u_k(x))\mathrm{d}x = \int_\Omega g(x) \int_{\mathbb{R}^{3\times 3}} \psi(x,A)\mathrm{d}\nu_x(A)\mathrm{d}x$. The set of all Young measures shall be denoted $\mathcal{G}^p$.

With the usage of Young measures we may introduce the relaxed Gibbs free energy $G(t,y,\nu,\lambda) = \int_\Omega \int_{\mathbb{R}^{3\times 3}} \varphi(A)\mathrm{d}\nu_x(A)\mathrm{d}x - \int_\Omega f(t,x)y(t,x)\mathrm{d}x - \int_{\Gamma_N} g(t,x)y(t,x)\mathrm{d}S$, where f is the volume force, whereas g the surface force applied on a part of the boundary Γ_N. Also, we may load the specimen by hard device by means of prescribing a Dirichlet boundary condition.

Related to the representation of microstructure with the help of Young measures is the notion of *volume fractions* a vector $\lambda \in \Lambda = \{\tilde{\lambda} \in \mathbb{R}^{M+1}, 0 \le \tilde{\lambda}_i \le 1 \text{ for all } i = 0 \dots M, \sum_0^M \tilde{\lambda}_i = 1\}$,

[a] e-mail: benesova@it.cas.cz

Article available at http://www.esomat.org or http://dx.doi.org/10.1051/esomat/200902003

representing the proportion of the respective martensite variants and the austenite phase in a selected material point, M is the number of martensitic variants. Naturally there has to be a relation between λ and ν which we write as $\lambda(x) = \int_{\mathbb{R}^{3\times 3}} \mathcal{L}(A)\mathrm{d}\nu_x(A)$, the function $\mathcal{L}$ has to be chosen constitutively, see e.g. [14,17,28].

It is known from experiments (cf. e.g. [26]) that the change of microstructure leads to dissipation, which for our considerations should be simplified to the statement that the change of volume fractions leads to dissipation that will be modeled phenomenologically (as already used in e.g. [14,25,28]). This is of course a rather strong simplification, which however allows us to use standard techniques in our modeling in the analytical as well as computational part. Agreeing on this assumption we may regard the vector of volume fractions as an internal parameter, the evolution of which is governed by the evolution inclusion $\mathrm{D}G(t,y,\nu,\lambda) + \partial R(\dot{\lambda}) \ni 0$, where R is the potential of dissipative forces, representing phenomenologically the effects on microscale responsible for dissipation; here we exploited the concept of *generalized standard solids* cf. [11, 10]. Standardly the dot denotes the derivative with respect to time, the symbol ∂ corresponds to the subdifferential of a convex function which we are entitled to use as R is assumed to be convex and D is the Gâteaux-derivate, which is used only formally as the smoothness of the Gibbs free energy is not guaranteed. Since we are able to write the evolution inclusion only formally, it is necessary to introduce a suitable weak solution of it, namely the *energetic solution*, first introduced by Mielke at. al. ([16,19,20]), which is suitable if $R(\cdot)$ is homogeneous of degree one i.e. the system is rate-independent.

Further denote $Q = \{(y,\nu,\lambda) \in W^{1,p}(\Omega,\mathbb{R}^3) \times \mathcal{G}^p \times L^\infty(\Omega,\mathbb{R}^{M+1}),\ \nabla y = \int_{\mathbb{R}^{3\times 3}} A\mathrm{d}\nu_x(A),$ $\lambda \in \Lambda, \lambda(x) = \int_{\mathbb{R}^{3\times 3}} \mathcal{L}(A)\mathrm{d}\nu_x(A)$ for a.a. $x \in \Omega\}$ the space of all admissible states. Then we may define an energetic solution as follows.

Definition 1 *The process $q : [0,T] \to Q$ is called an energetic solution to the SMA-problem, if it satisfies*

1. the stability condition*:*
$$G(t,q(t)) - G(t,\tilde{q}) \le R(\tilde{q} - q(t)) \tag{1}$$
for all $t \in [0,T]$ and all $\tilde{q} \in Q$,
2. the energetic equality*: whenever $q(t) \in Q$ then $\partial_t G(t,q(t))$ exists and is continuous and moreover*
$$G(t_2,q(t_2)) - G(t_1,q(t_1)) + \mathrm{Diss}_{[t_1,t_2]}(q(t)) = \int_{t_1}^{t_2} \partial_t G(t,q(t))\mathrm{d}t, \tag{2}$$
holds for all $0 \le t_1 \le t_2 \le T$. Here the total dissipation is defined as a variation over the dissipation distance in time i.e.
$$\mathrm{Diss}_{[t_1,t_2]}(q(t)) = \sup\left\{\sum_i R(q(t^{i+i}) - q(t^i));\ \text{of all partitions}\, t_1 \le t^1 \le t^2 \ldots \le t^n \le t_2\right\}.$$

To end this section let us just shortly note that, under the same growth and smoothness assumptions on the Gibbs free energy, the dissipation distance and the loads (as specified in [14,17] for zero Dirichlet-boundary conditions), the existence of energetic solutions can be guaranteed.

2 Time Discretization, Numerical Simulations

A significant advantage of the concept of energetic solutions is that it allows for a convenient time discretization, cf. [14,16,17,19]. Namely, the application of Rothe's method leads to the following time-incremental minimization problem. Let q_0 be the initial condition of the energetic process. Then when setting $q_N^0 = q_0$ we denote q_N^k the solution of

$$\begin{aligned} &\text{Minimize}\ \ G(t_k,\tilde{q}) + R(\tilde{q} - q_N^{k-1}) \\ &\text{subject to}\ \tilde{q} \in Q, \end{aligned} \tag{3}$$

where $0 = t_0 < t_1 < t_2 \ldots < t_{N-1} \leq t_N = T$ is some partition of the interval $[0, T]$.

This is indeed a good time-discretization as solution of the time-incremental problem really converge (under some appropriate data qualifications as specified in e.g. [14]) to an energetic solution. Our main concern throughout this section will nevertheless not be the proof of this convergence, but we shall focus on the numerical search of solutions to (3). The most intuitive way to do so is to implement directly (3) and perform the minimization by means of a gradient-type algorithm (e.g. L-BFSG-B [8,32] which was used to calculate the results presented in this contribution). However, what is demanded here, is the minimization of a cost-functional which has to be non-convex and non-smooth if we are modeling SMA. Furthermore the minimization includes up to several thousands degrees of freedom, which is very ambitious in global optimization. Still, especially for rate-independent processes we are able to design algorithms that search more effectively for global optima than a simple gradient-method-type algorithm.

These improved algorithms are based on a 0-order necessary (energetic) condition for (3) in time-step k as well as $k-1$ given in the following lemma (for a proof see e.g. [14,17,19]).

Lemma 1 (Two-sided energy inequality) *Suppose that q_N^k is a solution to (3). Then it satisfies, for all $k = 0, 1 \ldots N$, the discrete two-sided energy inequality*

$$\int_{t_{k-1}}^{t_k} \partial_t G(t, q_N^k) \mathrm{d}t \leq G(t_k, q_N^k) + D(q_N^{k-1}, q_N^k) - G(t_{k-1}, q_N^{k-1}) \leq \int_{t_{k-1}}^{t_k} \partial_t G(t, q_N^{k-1}) \mathrm{d}t. \qquad (4)$$

Roughly speaking, the violation of the lower inequality in (4) indicates that q_N^{k-1} is not a global minimum as q_N^k allows us to achieve a lower value in (3) (for the time-step $k-1$) while, on the other hand, the violation of the upper inequality shows that q_N^k is not a global minimum as q_N^{k-1} allows to us achieve a lower value in (3)(for the time-step k). This knowledge allows us to design an algorithm, referred in what follows to as the *backtracking algorithm*, that verifies the energy inequality and which is given in the block-diagram in Figure 1. Firstly, this algorithm has been used in [18](however in a much simpler problem of quasi-static damage) and we show its effectiveness in Figure 3. Let us just mention that a backtracking algorithm has also been used in [6,7], where however not the two-sided energy inequality but a different condition has been verified.

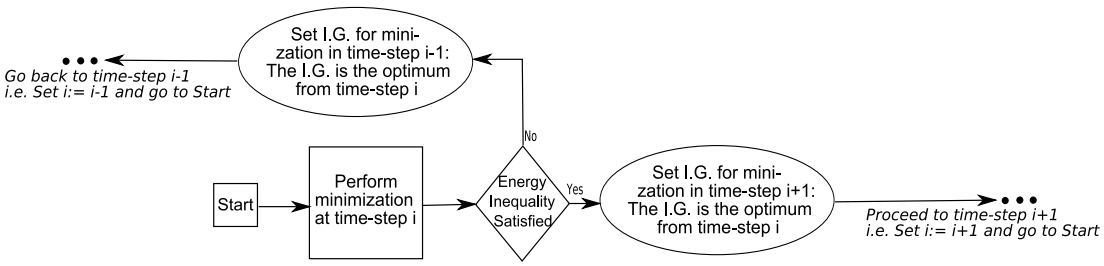

Fig. 1. A scheme of the strategy of backtracking shown on one specific time-step. The arrows show the proceeding of the algorithm, I.G. abbreviates initial guess.

Although the backtracking algorithm is effective on coarse meshes, on fine meshes it has serious difficulties. Therefore we developed a second algorithm based on a kind of a multigrid strategy. To be more specific, we first perform the whole calculation (by using the backtracking algorithm of course) on a coarse mesh. The results obtained there are extrapolated and given to the algorithm as initial guesses, when performing the calculation on a fine mesh. On the fine mesh we again use the backtracking strategy, which now however is more complicated due to the non-standard choice of initial guesses. The algorithm is given in block-diagram in Figure 2 and will be referred to as the *multigrid algorithm*.

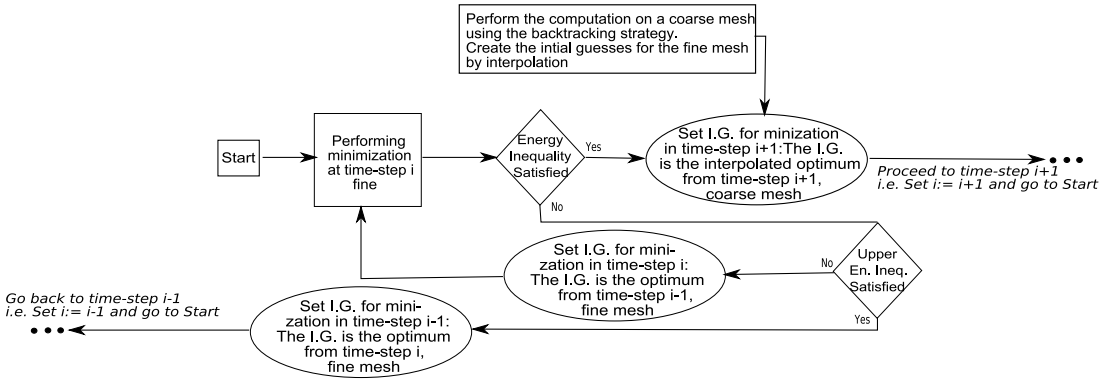

Fig. 2. A scheme of the multigrid strategy on one specific time-step. The arrows show the proceeding of the algorithm, I.G. abbreviates initial guess.

3 Illustration on a specimen of NiTi

We now present some numerical examples calculated with the help of the above algorithms performed on a single-crystal cuboid specimen of *NiTi*.

NiTi is a SMA which can be found in three different phases, the cubic austenite, the rhombohedric R-phase and the monoclinic martensite phase [24]. The transition from austenite to R-phase however can also be seen as a martensitic transformation as it manifests itself in changes of electric resistivity [31] or neutron diffraction measurements [29]. In this work we shall be concerned with pseudo-elasticity, in which a martensitic transition between the austenite and the R-phase occurs; the monoclinic martensite does not come into play. This is of course a simplification, as the behavior of the R-phase is most interesting in combination with a transition to the monoclinic martensite but, as we already pointed out, the modeling of SMA includes the minimization of a non-convex functional and hence including also the martensitic phase would complicate the situation and require further effort.

The constitutive choice for the stored energy for the calculations was chosen of a St.Venant-Kirchhoff type and also frame indifferent form to be

$$\psi = \min_{m=0\ldots4} \psi^m(F),\ \psi^m(F,\theta) = \frac{1}{2}\sum_{ijkl} \epsilon^m_{ij} C^m_{ijkl} \epsilon^m_{kl} + o^m,\ \epsilon^m = \frac{U_m^{-T} F^T F U_m^{-1} - \mathbb{I}}{2},$$

where $U_0 = \mathbb{I}$ and U_m are the distortion matrices of the variants of R-phase, C^m_{ijkl} are the elastic constants and o^m offsets of the particular phase. This choice of the stored energy assures the already mentioned multi-well character typical of SMA. The elastic constants for the simulations were taken from [24,29], unfortunately however up-to-now only the elastic constants for the austenite phase are available, so we used them also for the R-phase. The distortion matrices for the R-phase are taken from [12,29]. As far as dissipation is concerned, we assume that $R(\lambda) = (0.5\text{MPa})|\lambda_0|$, which reflects that the dissipation of the phase transition between austenite and R-phase is very small.

The simulation which we performed was the loading of the single-crystal *NiTi* austenite in oriented $(1,0,0)$ direction by a hard device in $(1,1,1)$ direction. Because of this load the specimen transforms first from austenite to a laminate (here considered of the second order) between austenite and R-phase twins and then detwins to a single variant of R-phase. Interestingly, during the loading experiment the normal of the laminate between austenite and the twinned R-phase changes (recall that we did not punish this behavior by dissipation) and due to this the stress decays during the transformation, see Figure 3(f).

In Figure 3 these simulation results can be seen; there the big cube on the left is the specimen, the lines on the specimen show its finite element meshing. The different gray-scales of the specimen correspond to the volume fraction of austenite in the specimen. Moreover the

microstructure, as reconstructed in one selected element, is shown in a separate cube. This microstructure is then again given in Figure 4 to show the computed laminate in more detail.

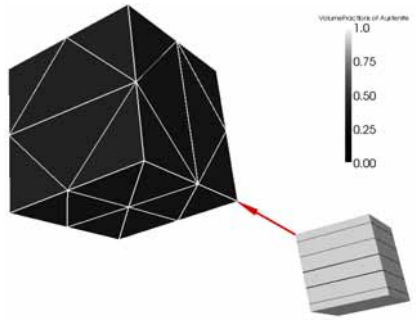

(a) Time-step 95, coarse mesh, no backtracking

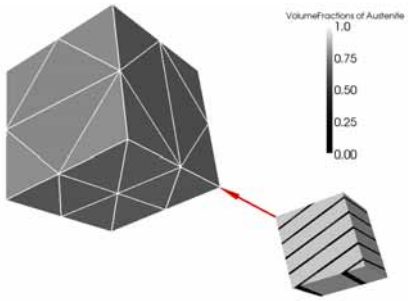

(b) Time-step 95, coarse mesh, backtracking

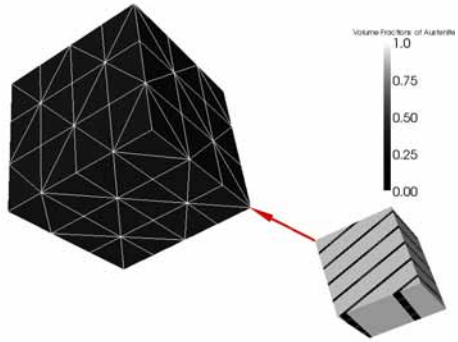

(c) Time-step 196, fine mesh, no multigrid

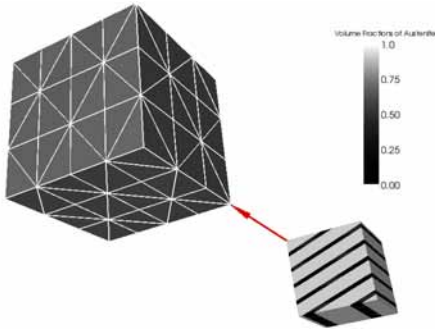

(d) Time-step 196, fine mesh, multigrid

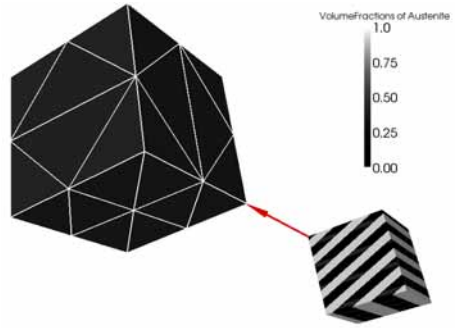

(e) Time-step 438, coarse mesh, backtracking

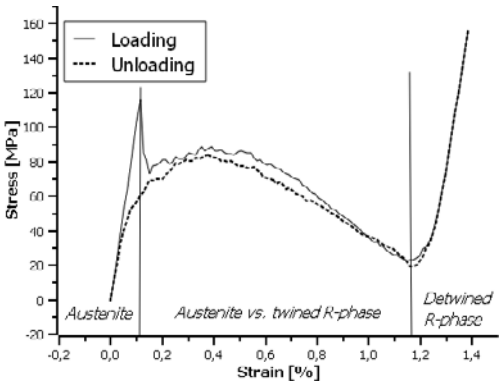

(f) Stress-strain diagram of a pseudoelastic evolution

Fig. 3. Simulation results when loading a $NiTi$ $(1,0,0)$-oriented single crystal undergoing a cubic-to-rhombohedric transformation in $(1,1,1)$ direction. Three specific time-steps out of 1000 for the whole calculation performed at transformation temperature and also a stress-strain diagram corresponding to the same loading but performend about transformation temperature are depicted here

These numerical results show that when not using the backtracking strategy on the coarse mesh the microstructure shown for one specific element and the volume fraction calculated there (on Figure 3(a)) do not agree (according to the volume fraction there is much less austenite than according to the microstructure), which shows that the calculated optimal state is in

some spinodal region where the relation $\lambda(x) = \int_{\mathbb{R}^{3\times 3}} \mathcal{L}(A)\mathrm{d}\nu_x(A)$ is far from being satisfied even approximately . This problem is resolved by using the backtracking algorithm. A similar situation encounters on the fine mesh, where only the multigrid strategy leads to good simulation results.

To end this section, let us give some notes on the spatial discretization of the problem. The displacement is approximated by element-wise linear function, which makes the deformation gradient element-wise constant. The microstructure (described by the gradient Young measure) is approximated by a laminate (as already in e.g. [2,13,14,28], some theoretical insight is given in [15]); here of the second order although theoretically a laminate of any order can be used in the code developed by the author.

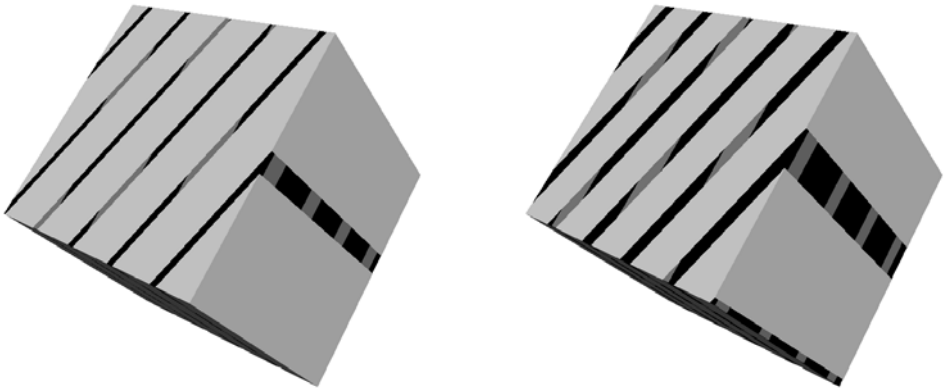

(a) Time-step 95 (b) Time-step 196

Fig. 4. Reconstruction of the microstructure from the same simulation as shown in Figure 3 on element zero (the same for which the reconstruction was shown also in 3) performed on a fine 180-element mesh.

Acknowledgment

This research was supported by the Nečas Center for mathematical modeling (project LC06052, financed by MŠMT), the project GACR 201/09/0917 and the research plan AVOZ20760S14. The author is also thankful to Martin Kružík and Tomáš Roubíček for their helpful comments on this paper.

References

1. M.Arndt, M.Griebel, V. Novák, T. Roubíček, P.Šittner, Int. J. Plasticity **22**, (2006) 1943-1961.
2. S. Aubri, M. Fago, M, Ortiz, Comp. Meth. in Appl. Mech. Engr. **192** (2003), 2823-2843.
3. J.M. Ball and R.D. James, Arch. Rational Mech. Anal. **100**, (1987) 13-52.
4. J.M. Ball and R.D. James, Phil Trans R Soc London A **338**, (1992) 389-450.
5. K. Bhattacharya, *Microstructure of Martensite. Why it Forms and how it Gives Rise to the Shape-Memory Effect* (Oxford University Press, New York 2003).
6. B. Bourdin, Interfaces Free Bound., **9** (2007),411-430.
7. B. Bourdin, G. Francfort and J.-J. Marigo, J. Elasticity **91** (2008),5-148.
8. R. H. Byrd, P. Lu and J. Nocedal, SIAM J. Sci. Stat. Comput., **16**, (1995) 1190-1208.
9. C. Carstensen, P. Plecháč, Math. Comp., **66**(1997), 997-1026.
10. K. Hackl, J. Mech. Phys. Solids, **45** (1997) 667-688.
11. B. Halphen, Q.S. Nguyen, J. Mécanique **14** (1975), 3963.
12. K.F Hane and T.W. Shield, Mater. Sci. Eng., A, **291**, (2000) 147-159.
13. M. Kružík, M. Luskin, Journal of Scientific Computing, **19** (2003), 293-308.
14. M. Kružík, A.Mielke and T.Roubíček, Meccanica, **40** (2005), 389-418.
15. M. Luskin, Acta Numerica, **5**, (1996) 191-258.

16. A. Mainik and A. Mielke, Calc. Var PDEs, **22** (2005), 73-99.
17. A. Mielke and T. Roubíček, Multiscale Model. **1** (2003), 571-597.
18. A.Mielke, T.Roubíček and J.Zeman, Computer Methods Appl. Mech. Engr., to appear.
19. A. Mielke and F. Theil, Nonl. diff, Eqns. Appl., **11** (2004), 151-189.
20. A. Mielke, F. Theil and V.I. Levitas, Arch. Rational Mech. Anal. **162** (2002), 137-177.
21. S. Müller, *Variational Models for Microstructure and Phase Transition* in S. Hildebrandt, M. Struwe(eds.), *Calculus of Variations and Geometric Evolution Problems (Cetraro, 1996)*, pp. 85-210, (Springer, Berlin, 1999).
22. M. Pitteri and G. Zanzotto, *Continuum Models for Phase Transition and Twinning in Crystals* (Chapman & Hall /CRC, Boca Raton 2003)
23. P. Pedregal, *Parametrized Measures and Variational Principles* (Birkhäuser, Basel 1997)
24. X. Ren, N. Miura, J. Zhang, K. Otsuka, K. Tanaka, M. Koiwa, T. Suzuki, Yu.I. Chumlyakov, and M. Asai, Mater. Sci. Eng. A,**312** (2001), 196-206.
25. K.R. Rajagopal, T. Roubíček, Nonlinear Anal., Real World Applications,**4** (2003), 581-597
26. K.R. Rajagopal, A.R. Srinivasa, Int. J. Plasticity **11** (1995), 653-678.
27. T. Roubíček, NATO Sci. Series II/170, Kluwer, Dordrecht, (2004), 269-304.
28. T. Roubíček, M.Kružík, J.Koutný, Proc. Estonian Acad. Sci. Phys. Math. **56** (2007), 146-154.
29. P. Šittner, D. Lugovyy, D. Neov, M. Landa, P. Lukáš and V. Novák, J. Phys. IV France, **112** (2003), 709-712.
30. C. Stupkiewicz. and H. Petryk, J. Mech. Phys. Solids, **50** (2002), 23032331.
31. J. Uchil, K.K. Mahesh, K. Ganesh Kumara, Physica B, **324** (2002) 419-428.
32. C. Zhu, R. H. Byrd and J. Nocedal, ACM Trans. Math. Softw., **23** (1997), 550-560